ELSEVIER

Contact pressure models for spiral phyllotaxis and their computer simulation

Heino Hellwig[a,*], Ralph Engelmann[a], Oliver Deussen[b]

[a]*Department of Computer Science, Dresden University of Technology, D-01062 Dresden, Germany*
[b]*Department of Computer Science, Konstanz University, D-78457 Konstanz, Germany*

Abstract

We present a simple, biologically motivated model for the creation of phyllotactical patterns in capitula and their computer simulation. An in-depth investigation of Ridley's contact pressure model is performed and a refinement of contact pressure between primordia on the basis of local centroidal Voronoi relaxation is presented. Using this method in combination with Hofmeisters rule for placing new primordia creates stable patterns with Fibonacci spirals of high degree for a large range of initial conditions.
© 2005 Elsevier Ltd. All rights reserved.

1. Introduction

Phyllotaxis describes the arrangement of repeated units such as leaves, steams, seeds in living plants. The early developmental stage of these units are called *primordia*. In many flowering plants specific patterns for the petals and seeds can be observed and many simulation methods have been published in order to explain their appearance. We provide a critical look at Ridley's (1982) contact pressure model and present some important extensions. Using these extensions we are able to simulate the genesis of higher-order patterns from the Fibonacci series. These patterns arise for a wide variety of starting configurations that are biologically plausible. To prove this, we use the so-called Hofmeister (Hofmeister, 1886) rule as a simple, biologically motivated insertion mechanism for new primordia.

Primordia are formed at the rim (the so-called *apical ring*) of the growing tip (*meristem*) and subsequently move radially outwards. Two main phyllotactic patterns can be distinguished: the *alternate patterns* with one leaf per node

and the *whorled patterns* having two or more leaves per node. The alternate patterns are often called spiral patterns and are the subject of our investigation. When only one primordia is formed at each time step (*monojugate spiral systems*), the spiral resulting from connecting these successive organs is called the *genetic* or *growth spiral*. In most of the flowering plants and conifers (Snow, 1955) one observes *secondary* spirals or helices, where the number of visible spiral arms in clockwise or counter clockwise direction (the so-called *parastichy numbers*) is given through successive numbers from the Fibonacci series $(1, 2, 3, 5, 8, 13, 21, 34, \ldots)$ (i.e. *Helianthus annes*). Other parastichy numbers are out of the first accessory series (Lucas series) $(1, 3, 4, 7, 11, \ldots)$ (i.e. *Araucaria excelsa, Euphorbia biglaendulosa*). In rare cases higher accessory series such as $(1, 4, 5, 9, 14, \ldots)$ or $(1, 2, 5, 7, 12, \ldots)$ can be found (Jean, 1994; Snow, 1955).

The divergence angle $\alpha = 2\pi\theta$ describes the angle between two successive primordia. Every positive real number $\theta \in \mathbb{R}$ can be expanded uniquely as a continued fraction (Khinchin, 1964):

$$\theta = [a_0; a_1, a_2, a_3, \ldots] := a_0 + \cfrac{1}{a_1 + \cfrac{1}{a_2 + \cfrac{1}{a_3 + \ldots}}} \qquad (1)$$

---

*Corresponding author. Tel.: +49 351 4671680.
E-mail addresses: hh10@inf.tu-dresden.de (H. Hellwig),
deussen@inf.uni-konstanz.de (O. Deussen).

Table 1
Some noble angles and the corresponding continued fractions

Degrees	θ	Continued fractions	Parastichy numbers
54.396..	$\dfrac{1}{5+\tau}$	$[0; 6, \bar{1}]$	$(1, 6, 7, 13, 20, 33, 53, \ldots)$
64.079..	$\dfrac{1}{4+\tau}$	$[0; 5, \bar{1}]$	$(1, 5, 6, 11, 17, 28, 45, \ldots)$
77.955..	$\dfrac{1}{3+\tau}$	$[0; 4, \bar{1}]$	$(1, 4, 5, 9, 14, 23, 37, \ldots)$
99.501..	$\dfrac{1}{2+\tau}$	$[0; 3, \bar{1}]$	$(1, 3, 4, 7, 11, 18, 29, \ldots)$
137.507..	$\dfrac{1}{1+\tau}$	$[0; 2, \bar{1}]$	$(1, 2, 3, 5, 8, 13, 21, \ldots)$
151.135..	$\dfrac{1}{4-\tau}$	$[0; 2, 2, \bar{1}]$	$(1, 2, 5, 7, 12, 19, 31, \ldots)$

for positive integers $a_0, a_1, a_2, a_3, \ldots$. The quantity obtained by including n terms of the continued fraction

$$\frac{P_n}{Q_n} = [a_0; a_1, a_2, a_3, \ldots, a_n] \qquad (2)$$

is called the nth convergent.

It is well known (Coxeter, 1972; Adler, 1998; Marzec and Kappraff, 1983) that most of the observed parastichy numbers are the denominators of the continued fractions convergent from noble divergence angles (see Table 1). A noble number is a quadratic irrational number having a continued fraction that becomes an infinite sequence of ones at some point.

Specially the Fibonacci numbers arise when the divergence angle is near the Golden Angle $\theta_G = 2\pi/(1 + \tau)$ radians (or $\approx 137, 507 \ldots$ degrees), where

$$\tau = \frac{\sqrt{5} + 1}{2} = 1 + \cfrac{1}{1 + \cfrac{1}{1 + \cfrac{1}{1 + \ldots}}}$$

is the golden mean.

In whorled patterns with parastichy numbers $k(i, j)$, $i \neq j$ there are multiple (k-jugate, $k \geqslant 2$) spiralsystems. Well known is the double-spiral type $(2, 4, 6, 10, 16, 26, 42, \ldots)$ (main Fibonacci bijugy), which occurs in 5.2% of the plants with spiral patterns (Jean, 1994).

Many causal models for the emergence of these patterns were developed. For an overview see Adler et al. (1997), Jean (1994), Jean and Barabe (1998). The mathematical modeling of the phyllotaxis must model two biological processes: firstly the processes inside the meristem which lead to the birth of the primordia at some decisive places and secondly the interaction of the primordia during their growth processes on the receptacle. The complete biological processes in the shoot apex are still unknown, however, a number of models have been presented that to a certain extent describe the processes.

To model the biological processes for the formation of primordia, Schoute (1913) developed the so-called inhibitor theory. It suggests that each new primordium produces a diffusing inhibitor which prevents the formation of new primordia until the concentration of the inhibitor is less than a critical threshold. This theory was developed further by Turing (1992) into a reaction–diffusion model. Different authors (Bernasconi, 1994; Koch et al., 1998; Meinhardt, 2003) enhanced this model type, however, their stability and convergence properties must be further investigated since in many cases these models achieve good results only for very exact starting configurations that cannot be provided by real plants. Furthermore, the chemical inhibitor substances are purely hypothetical.

The second process that is needed to form phyllotactical patterns are contact-pressure models which describe the interaction of the primordia during their growth on the receptacle. Corresponding models expect that the primordia touch each other at least in some phases of the growth process (Schwendener, 1878). The resulting contact pressure moves the primordia in positions of the largest possible distance to each other. An important work with amazing results for the investigation and simulation of such models was given by Ridley (1982). It is the basis of our contribution.

As mentioned above, our extensions of his model enables us to simulate the genesis of higher-order patterns of the Fibonacci series and the main Fibonacci bijugy $(2, 4, 6, 10, 16, 26, \ldots)$, which includes also the fluctuations of the divergence angle observed by Ryan et al. (1991) at, i.e. *H. annuus*. Using the Hofmeister rule for insertion we are able to vary the insertion angle without changing the final pattern. If, however, the pattern changes, typical other patterns that can be found in nature arise.

In the following section first Ridley's simulation method is sketched. In Section 3 we describe our new contact pressure computation using Voronoi diagrams. In Section 4 the Hofmeister rule is introduced and subsequently results are given.

2. The computer simulation of Ridley

In 1979 Vogel (Vogel, 1979) provided a simple mathematical description of the sunflower spiral pattern that encompasses the dense distribution of primordia as well as their regular arrangement on the receptacle. The position of the ith primordium $P_i, i \in \mathbb{N}$ is described in polar coordinates $(r_i, \alpha_i) = (c \cdot \sqrt{i}, 2\pi \cdot \theta \cdot i)$, with a constant $c \in \mathbb{R}_{\geqslant 1}$ and a constant divergence angle $2\pi \cdot \theta$, where $\theta \in \mathbb{R}, 0 \leqslant \theta < \frac{1}{2}$. The increase of the radius in form of a square-root is needed for the dense distribution on the receptacle.

Choosing the Golden Angle $\theta_G = 2\pi/(1 + \tau)$ as divergence angle results in the most uniform arrangement of the primordia on the circle. This was conjectured first by Steinhaus (Marzec and Kappraff, 1983). The insertion process on the circle given by $\alpha_i = (2\pi/(1 + \tau)) \cdot i$ is termed the Golden Algorithm (Dixon, 1983) and the resulting partition of the circumference was investigated thoroughly by Marzec and Kappraff (1983) and van Ravenstein (1989).

Ridley (1982) extended Vogels model in order to investigate a more complex contact pressure model given by Adler (1974) for the disc. Ridley made the assumption that, whatever the mechanism for determining the birthplace of a new primordia may be, it will place the next primordium at a certain angle from its predecessor. However, it is unlikely that a plant is able to do so with the incredible accuracy displayed in the final capitulum. For various divergence angles at the start his computer simulation showed a fast convergence of the mean of the divergence angles to the Golden Angle with very small standard deviation. The most remarkable result of his investigations was a self-organizing property of the contact pressure in combination with his birthplace calculation. Such a self-organizing property is necessary since the apex ring was build out of not more than 100 cells which implies that the location of the primordia birthplace cannot be determined with greater precision than 3.6° (Koch et al., 1998). Apart from that there are thermodynamical, biochemical and mechanical effects during the growing process. The question about the origin of this self-organizing property and the allowed range of mean and standard deviation of the initial divergence angles necessary for producing high-order Fibonacci phyllotaxis was not investigated so far.

2.1. Simulating contact pressure

Ridley's simulation of the contact pressure on a disc consists of the following three steps (see Ridley (1982) for details and also the pseudo-code in Appendix A):

(1) *Forming a new primordium*: Equal time steps between the forming of new primordia are assumed. At each time step a new item P_i represented by a circle of radius $\varrho = 1$ is formed on the rim of an unit circle according to a special generation procedure (see below).
(2) *Interaction of the existing primordia*: After the genesis of a new primordium the contact pressure and resulting movement is computed between all existing primordia and their neighbors. Doing so, under some special restrictions for the movement a rearrangement of the primordia is formed. This procedure is repeated a specific number of times before the expansion of the capitulum, Ridley calls each of the movements a wave (for details see Section A.1).
(3) *Expansion*: After applying the contact pressure, all existing primordia receive a radial expansion $r_i \rightarrow \sqrt{r_i^2 + 1}$. This leaves a gap for a new primordia near the center.

To motivate our improvements of Ridley's simulation model given in the next section, we first analyse the results that are achieved with his simulation for a number of initial conditions. Firstly, we investigate two different kinds of

generation procedures:

(a) Provided, a new primordium P_i is set with a preassigned divergence angle. Here is assumed that the insertion processes in the apex-ring are independent of the position of the older primordia on the receptacle. That assumption was made for example implicitly by Bernasconi (1994) and Koch et al. (1998). They investigated reaction–diffusions models with three chemical substances on a one-dimensional segment of unit length with periodic boundary conditions. For a special parameter selection they achieve an activator maximum at an divergence angle near the Golden Angle.
(b) Provided, a new primordium P_i is set with divergence angles that are obtained from the adjusted position of the preceding item P_{i-1} *after* contact pressure movements. That was part of Ridley's (1982) original simulation motivated by the fact that biologists expect an interaction between existing and new primordia (Kuhlemeier and Reinhardt, 2001; Schoute, 1913; Stieger et al., 2002). Ridley therefore applies his initial divergence angles always between the position of the youngest primordium, that was already pushed due to contact pressure simulation a number of times, and the birthplace of the next primordium.

2.2. Results of the computer simulations

2.2.1. Simulations with preassigned divergence angles

Using an preassigned input sequence we achieve the following measurements:

(i) For a constant preassigned input-divergence-angle between the primordia birthplaces we find no convergence to the Golden Angle for the mean divergence-angle in capitula with 500 primordia. Instead the mean nearly equals the provided input angle for a large interval. The standard deviation shows minima at the Noble numbers $\alpha = 1/(t + \tau)$, with $t \in \mathbb{N}$. This reflects the even distribution of points in so-called Golden Lattices (Marzec and Kappraff, 1983, see Theorem 9). In Fig. 1 this can be observed.
(ii) In the case of normal distributed input-divergence-angles $\alpha \in N(\theta_G, \sigma)$ with golden mean $\mu = \theta_G$ and standard deviation $\sigma \in [0°, 20°]$ we measured a significant decrease of the standard deviation σ in the region $[0°, 6°]$. The mean angle, however, stays constant at θ_G. Fig. 2 shows the effect.

2.2.2. Ridley's simulation

The divergence angles are measured from the adjusted position of the preceding primordium *after* contact pressure movements. In this case our results are the following:

(i) We made a simulation with 300 primordia, a wave number of 3 (the number of interactions between the
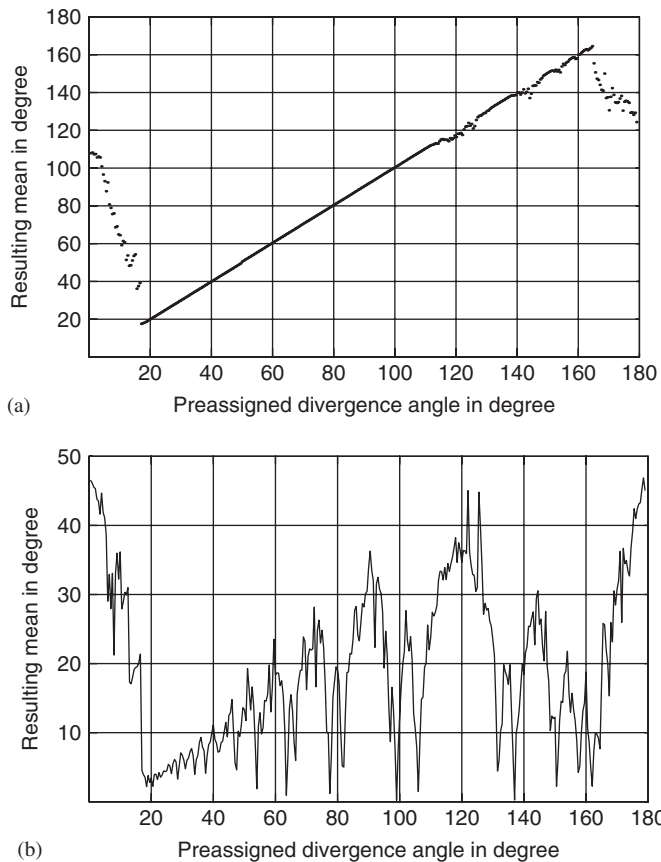
Fig. 1. Resulting (a) mean μ and (b) standard deviation (SD) σ for 500 primordia in dependence to a constant preassigned divergence angle between primordia birthplaces.
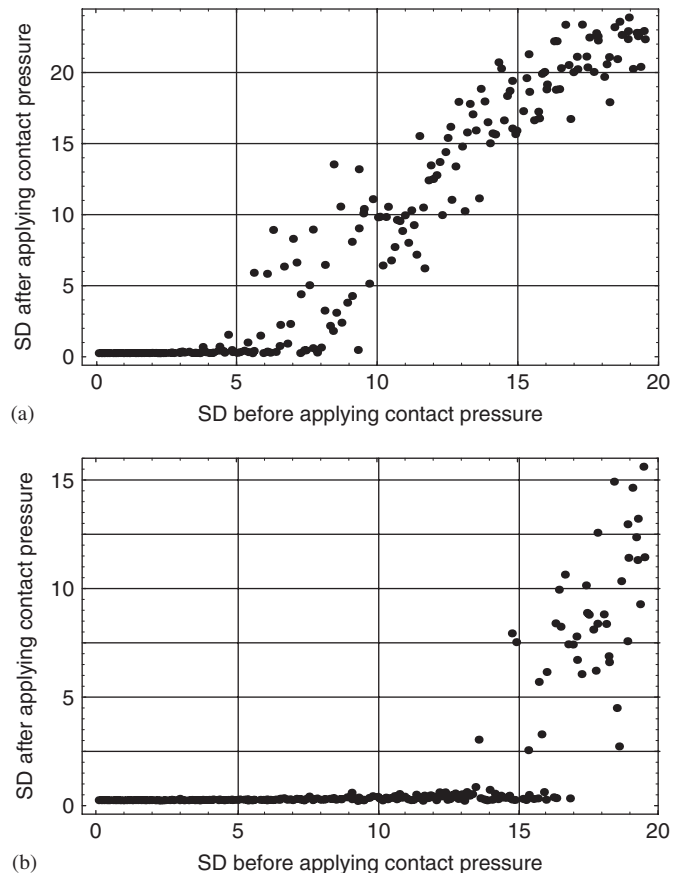

Fig. 2. (a) Standard deviation (SD) σ after contact pressure simulation in capitula with 500 primordia, in dependence on the SD σ of a normal distributed $N(\theta_G, \sigma)$ preassigned divergence angle sequence before contact pressure. (b) The same measure for divergence angle sequence measured from the adjusted position of the preceding primordium *after* contact pressure movements.

primordia before the next insertion) and a movement limitation of 0.1 units per step. In this case, for a constant input-divergence-angle the resulting mean angle over a wide range of initial angles is a quasi-discrete function with values near the Golden Angle, the Lucas angle and the noble angle $77.95°$. Input angles between $127°$ and $149°$ resp. between $83°$ and $101°$, produce a mean near the Golden Angle resp. the Lucas angle. For input angles between $132°$ and $148°$ resp. between $84°$ and $97°$ the standard deviation is smaller than $1°$. Fig. 3 displays these results.

Outside of these ranges the standard deviation is much higher, meaning that the associated spiral pattern has defects or does not arise at all (see Fig. 4(a)). Remark that some of these defects could not be observed by Ridley since his measures were limited to 100 primordia and these defects often arise only beyond that limit. If the wave number increases to 5 some defects disappear (see Fig. 4(b)). If the movement limitation is increased to 0.3, also the noble angles $64.08°$ and $151.14°$ appear as stages in the resulting mean value diagram.

(ii) For normal distributed input-divergence-angle with mean μ and standard deviation $\sigma \in [0°, 20°]$, Fig. 2 (bottom row) shows that the range of input angles that result in a very small final standard deviation is now significantly larger with $\sigma \in [0°, 15°]$.

In this way our simulations confirm Ridley's results for the most part and answer the question for which divergence angles a self-regulation appears.

In the following we go further and present a refined model. The contact pressure processes is now simulated through a local centroidal Voronoi relaxion. Furthermore, we simulate the formation of the primordia according to Hofmeisters rule (Hofmeister, 1886), which states that a new primordium is formed at the place where the distance to the already existing primordia reaches a maximal value (cf. also Atela et al., 2002; Snow, 1955).

3. Simulation using centroidal Voronoi relaxation

Until now in phyllotaxis research Voronoi regions[1] were solely used for analysing several models (Dixon, 1998; Rivier et al., 1984; Rothen and Koch, 1989). As an example, Richards (1948) constructed a Voronoi tessellation for a set of points which were placed using the Golden Angle θ_G and a radial expansion coefficient $H = r_{i-1}/r_i$ to

---

[1]For a short description of Voronoi regions see Appendix B.
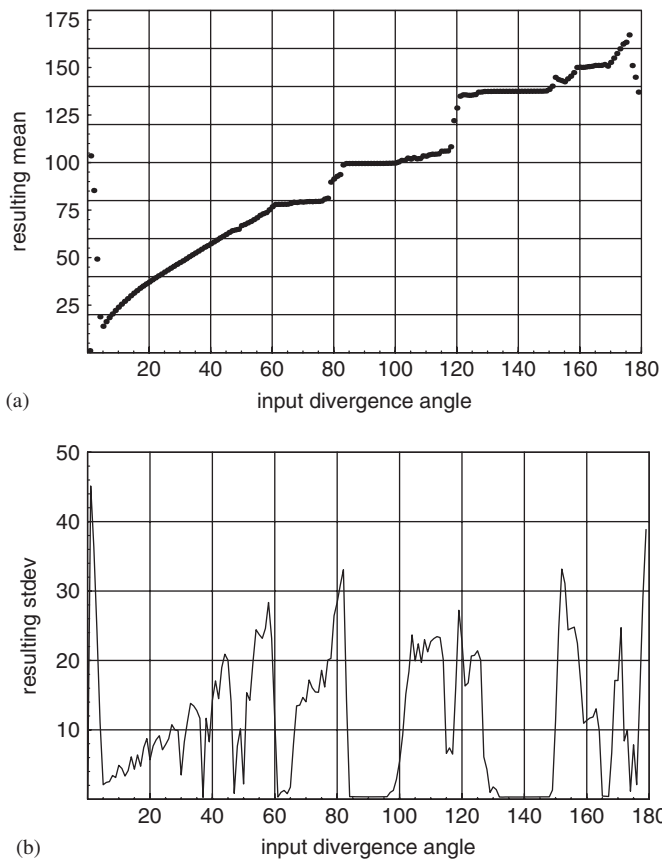
(a)

(b)

Fig. 3. (a) Mean μ and (b) SD σ in capitula (300 primordia) resulting from Ridley's contact pressure simulation (3 waves, movement limit 0.1).

visualize the uniform placement of the points on a disc. Rothen and Koch (1989) showed that the form deformation of a Voronoi region of a lattice grid on a growing cylinder is minimal for noble divergence angles.

We propose a complementary approach: the alteration of the form during the simulation of contact pressure is minimized using a centroidal Voronoi relaxation. That means we compute the Voronoi regions of all primordia epicenters and move these points to the centroids of their Voronoi regions (for details see Section B.2). This is repeated a number of times (this number is equivalent to the wave number in Ridley's simulation). Doing so, we are able to accurately compute the forces an elastic primordium receives due to the contact pressure of its neighbors. In Fig. 5(a) a point set with its Voronoi diagram (the conjunction of all Voronoi regions) is shown, in (b) we see the path of the points during the relaxation, subfigure (c) shows the final positions.

The simulation of contact pressure using a centroidal Voronoi relaxation is biological plausible as was shown by Honda (1978, 1983) who measured the positions of cells to be a centroidal Voronoi partitions for a number of cell tissues. Due to the restrictions of movements on cell tissues and the finite influence of the contact pressure we replace in the construction of the Voronoi regions the half-spaces that have to be intersected (see Appendix B) by circles with a
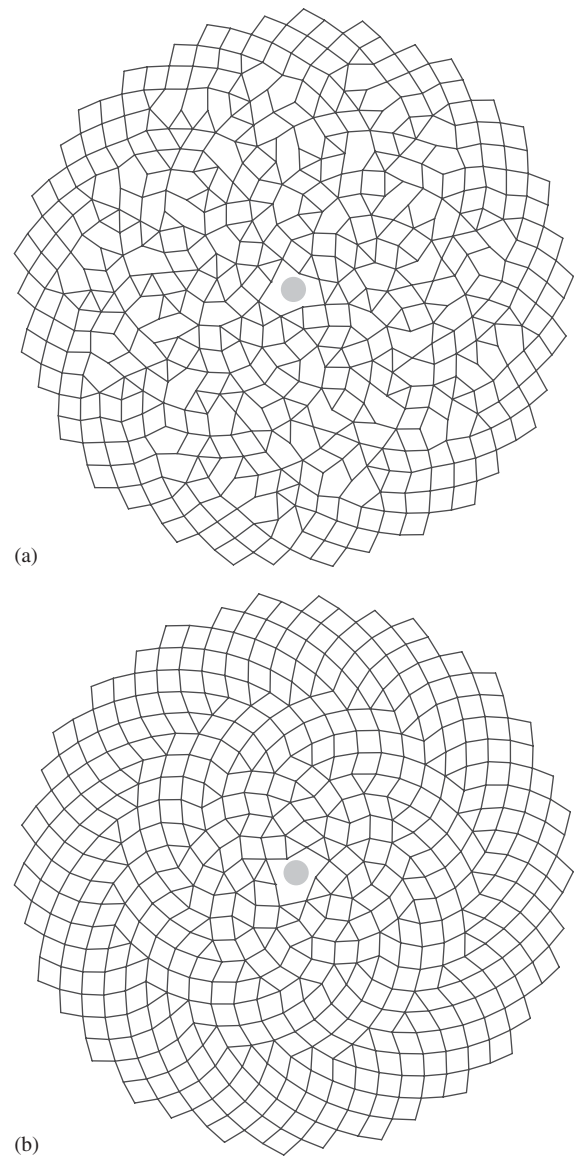

(a)

(b)

Fig. 4. Capitulum (500-Primordia) resulting from a Ridley-simulation with input angle 131° and (a) 3 waves (resulting mean $\mu = 137,42°$, $\sigma = 1,842°$). Only the (34,55)-Parastichies are visible. (b) 5 waves (resulting mean $\mu = 137,507°$, $\sigma = 0,296°$). Now the (13,21,34,55)-Parastichies become visible.

radius $\varrho = 1$. This limits the size of the primordia and lets them behave like small circular elements. In Fig. 6 we show the effect: in the inner part of the pattern, the Voronoi cells have a polygonal outline, in the outer part the cells are represented as circles. We call the centroidal Voronoi relaxation base on this variation a *Local centroidal Voronoi relaxation* (LCVR).

To introduce this new form of contact pressure in Ridley's algorithm we have to change the following (cf. Section B.2): if the circles which represent the primordia overlap, we moving each center to the centroid of its Voronoi region. This procedure is iterated a number of times before the next primordium emerges. An easy calculation show that the displacement $0.5 - 0.25 \cdot k$, where
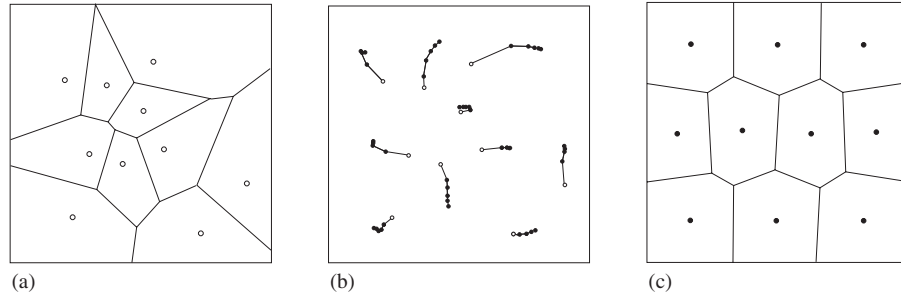
Fig. 5. Centroidal Voronoi relaxation: (a) initial positions with Voronoi diagram; (b) path of the positions during relaxation; (c) final positions after 50 steps.

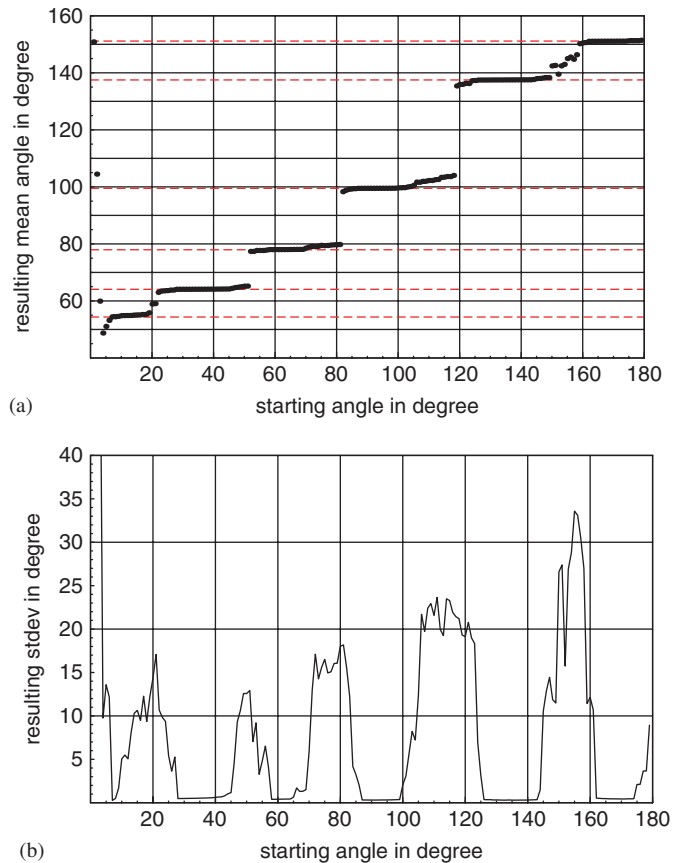Fig. 6. Local centroidal Voronoi relaxation.

Fig. 7. (a) Mean μ and (b) SD σ in capitula (300 primordia) resulting from contact pressure simulation with a LCVR (movement limit: 0.3, relaxation depth: 3, $\varepsilon = 0.03$).

$k < 2$ is the distance between the centers of two overlapping primordia, used by Ridley is a good approximation of this centroid-displacement when only two circles are in contact. If more circles overlap there is no easy analytical description of the resulting displacement. In this case we compute the local Voronoi tessellation of the whole set approximately by using simple algorithmic geometry (Bashein and Detmer, 1994).

Replacing Ridley's replacement function through the one resulting from a LCVR, we get a resulting mean diagram similar to Fig. 3(a). Also the resulting SD diagram looks like Fig. 3(b), however, the valleys near the noble angles are significantly smaller. Increasing the movement limitation to 0.3 units (cf. Fig. 7) the staircase form of the mean-diagram is now much clearer and the other nobel angles $64.08°$ and $54.36°$ become visible. When we increase the number of waves to 7 a more characteristic step function appear, but the smallest step at $54.36°$ disappears.

Remark that Ridley's contact pressure computation produces nearly the same diagrams for a movement limitation of 0.3 units. A significant difference will appear in the next section.

4. Hofmeister hypothesis

Let us now come to the other part of the simulation. We replace Ridley's primordia input procedure by the so-called Hofmeister rule. In 1868, the botanist Hofmeister

established, based on microscopic observations, an important hypothesis about the primordia formation at the shoot apex (Hofmeister, 1886): *Es ist eine durchgreifende Erfahrung, dass neue Blätter (oder Seitenachsen) an denjenigen Orten über den Umfang des im Zustande des Vegetationspunktes befindlichen Stängelendes (oder Stängelgürtels) hervortreten, welche am weitesten von den Seitenrändern der Basen der nächstbenachbarten, bereits vorhandenen Blättern entfernt sind.* (Hofmeister, 1886, pp. 482–483.) Many experiments done by Snow and Snow (Snow, 1955) and others supported this hypothesis. Snow and Snow (Snow, 1952) extend this to the so-called space-filling-theory, which first was mathematical investigated by Adler (1975). The Hofmeister rule was also used 1996 by the physicists Douady and Couder (1996) to make numerical simulations of their famous experiment, which used drops of magnetic ferrofluids to simulate the repulsion forces between the primordia. Based on this work Atela et al. (2002) presented a discrete dynamical system to investigate the influence of Hofmeister's rule in pattern formation. They were able to make a rigorous mathematical analysis and proved that the fixed points in this system are helical lattices, which are asymptotically stable.

Recent advances in the study of the growth hormone Auxin (Flemming, 2005; Kuhlemeier and Reinhardt, 2001; Stieger et al., 2002) supports this view. It was shown that the forming of new leaves acts as sinks for the Auxin. As a consequence, the Auxin concentration in the apex ring is assumed to be highest at the position on the apex which is most far away from the already existing primordia. It is plausible that a new primordium is then placed in conformity to the Hofmeister hypothesis.

The Hofmeister rule can be easily implemented in Ridley's contact pressure model. Therefore, we divide the ring on which the primordia appear in equal pieces. We perform our simulations with 100, 360, 3600 intervals reflecting an scan-angle of 3.6°, 1° resp. 0.1°. The results are qualitatively similar. For the diagrams we use the scan-angle 0.1°. Then we compute for each of the resulting equidistant points the minimum distance to the set $S = \{P_i\}_{i=1,\dots,n}$ of already existing primordia. The primordium P_{n+1} is then placed at the position with the largest minimal distance, the so-called MaxMin-principle (Adler, 1974).

In most botanical cases, already existing axillary buds or other lateral appendages such as cotyledons (Douady and Couder, 1996, p. 265) might force a inhomogeneous initial Auxin distribution in the meristem that causes an unsymmetrical position of the first formed primordia. Such unsymmetrical starting position were already expected in other models (Williams and Brittain, 1984, p. 66; Douady and Couder, 1996, p. 260). We simulate this initial situation using default positions of the first two primordia P_1 and P_2 (see Figs. 8 and 9). Fig. 8 reflects the geometrical situation in absence of contact pressure. Fig. 9 shows the same situation with Ridley's contact pressure calculation. Interestingly, for different initial angles the resulting mean angles are close to one of the three types: the Golden
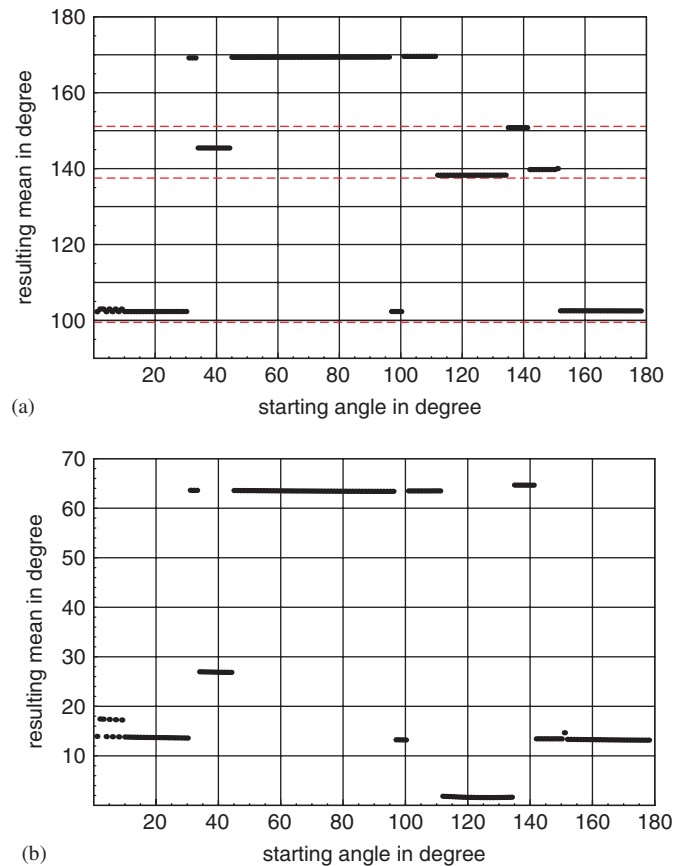

(a)

(b)

Fig. 8. (a) Mean μ and (b) standard deviation σ (bottom) in capitula (500 primordia) resulting from the Hofmeister rule in dependence of a default starting angle without any contact pressure.

Angle, the Lucas angle or a periodic orbit. For starting angles α between $75° < \alpha < 92°$ and $109° < \alpha < 111°$ the Hofmeister rule leads to a periodic two-input-sequence with angles near $(123°, 173°)$. For starting angles between $93° < \alpha < 108°$ we receive a periodic four-input-sequence with angles near $(100°, 200°, 280°, 190°)$. Furthermore, it can be observed that the contact pressure enlarges the initial values leading to the Golden Angle from the two segments $112°–134°$ and $141°–151°$ to a large segment $112°–178°$.

In simulations that combine the Hofmeister rule, the LCVR and a default starting angle we obtain a quite different diagram (see Fig. 10), showing the influence of the contact pressure function. For starting angles α between $18° < \alpha < 52°$ the resulting configuration is mostly the main Fibonacci bijugy. For starting angles α between $111° < \alpha < 151°$ the resulting configuration is the Fibonacci-spiralsystem .

If the relaxation deep increase to 10 we obtain diagram Fig. 11. For starting angles α between $21° < \alpha < 78°$ the resulting configuration is the Lucas-spiralsystem (cf. Fig. 12b). For starting angles α between $79° < \alpha < 98°$ and $112° < \alpha < \approx 155°$ the resulting configuration is the Fibonacci-spiraltype (cf. Fig. 12a). For starting angles α
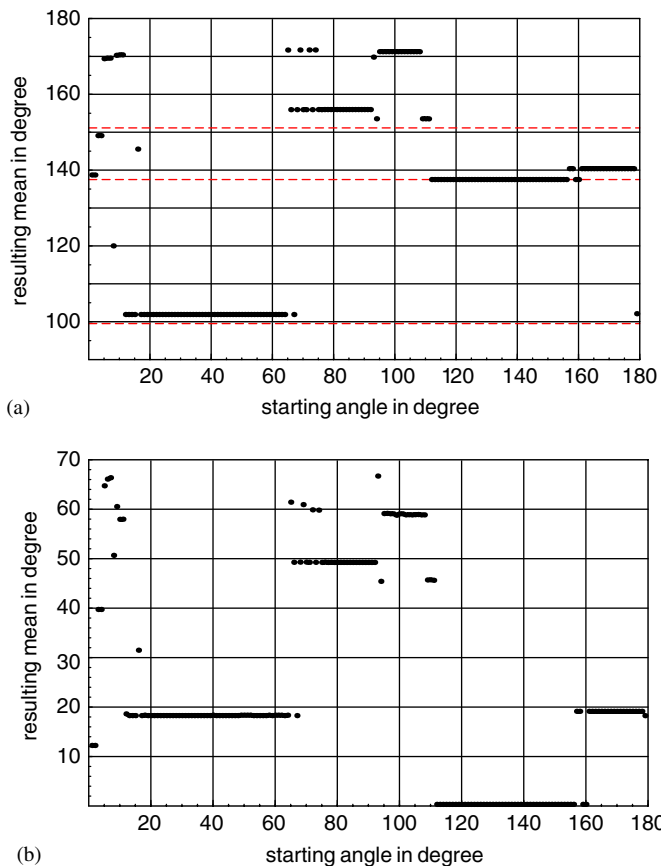
Fig. 9. (a) Mean μ and (b) SD σ in capitula (300 primordia) resulting from a contact pressure simulation with the Hofmeister rule and Ridley's contact pressure calculation in dependence of a default starting angle (movement limit: 0.3, wave number: 3).
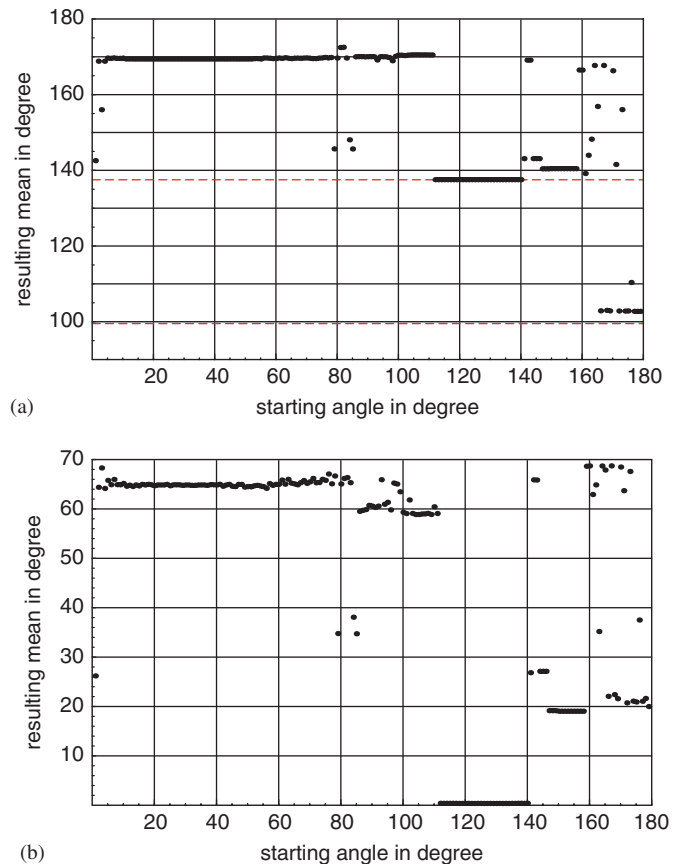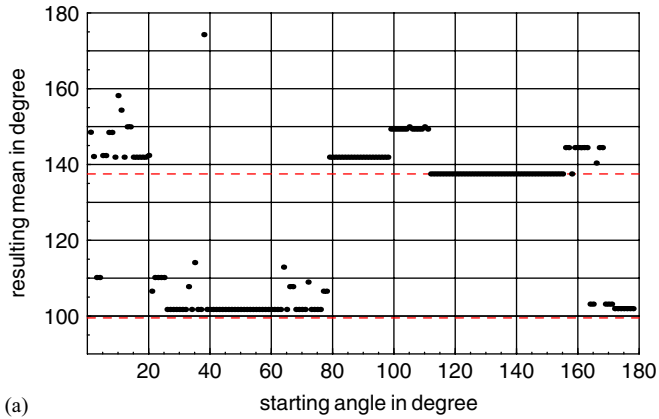

Fig. 10. (a) Mean μ and (b) SD σ in capitula (300 primordia) resulting from a contact pressure simulation with the Hofmeister rule and LCVR in dependence of a default starting angle (movement limit: 0.3, relaxation depth: 3, $\varepsilon = 0.03$).

between $99° < \alpha < 111°$ the resulting configuration is the main Fibonacci bijugy (cf. Fig. 13).

This is interesting since it seems to be plausible that in nature plants are only able to position their primordia within such a large interval. Furthermore, the resulting patterns are stable against perturbations of the computed input positions. Another interesting property of our simulation is the permanent fluctuations of the divergence angle as shown in Fig. 14. This diagram looks very similar to the one measured by Ryan et al. (1991) at *H. annuus*. Also make aware that the Fibonacci series, the Lucas series and the main Fibonacci bijugate are the most frequently observed patterns at *H. annuus* (Jean, 1994; Schoute, 1938).

5. Summary and future work

Phyllotaxis is a very complex phenomenon which is determined by many parameters. A single model alone can surely explain only some of the aspects of the underlying biological processes. The presented model refines Ridley's contact pressure method. It supports the positioning of the primordia following the Hofmeister rule. For a large interval of starting angles our simulation produces a quick convergence to the Golden Angle with small standard

deviation. This enables us forming patterns with higher-order Fibonacci parastichies. Furthermore, our model demonstrates the influence of the repulsion function and the starting conditions to the simulation. It is easy to implement further variations such as age-dependent relaxation depth and/or direction-dependent movement limitations. For supporting these modifications there is a great need for empirical studies. We need more information about the biological realization of the Hofmeister rule and about the repulsion forces between primordia.
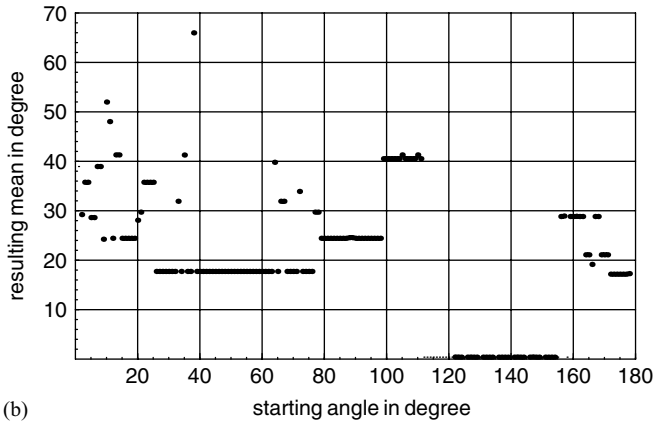
In future work we want to investigate the influence of growing primordia on the contact-pressure model for a plane capitulum and for a more biologically plausible capitulum in the shape of an arbitrary surface of revolution (Ridley, 1986). Furthermore, the hypotheses of Snow and Snow (Snow, 1952) should be investigated that states that new primordia appear when and where large enough space has been formed at the periphery of the apex.

Our model assumptions are still quite idealistic. However, we hope that our contribution demonstrates the relevance of a dynamical system that combines the Hofmeister rule with contact pressure simulation and that it helps biologists in receiving a better understanding of these beautiful plant patterns.

Fig. 11. (a) Mean μ and (b) SD σ in capitula (300 primordia) resulting from a contact pressure simulation with the Hofmeister rule and LCVR in dependence of a default starting angle. Movement limit: 0.3, relaxation depth: 10, $\varepsilon = 0.01$.

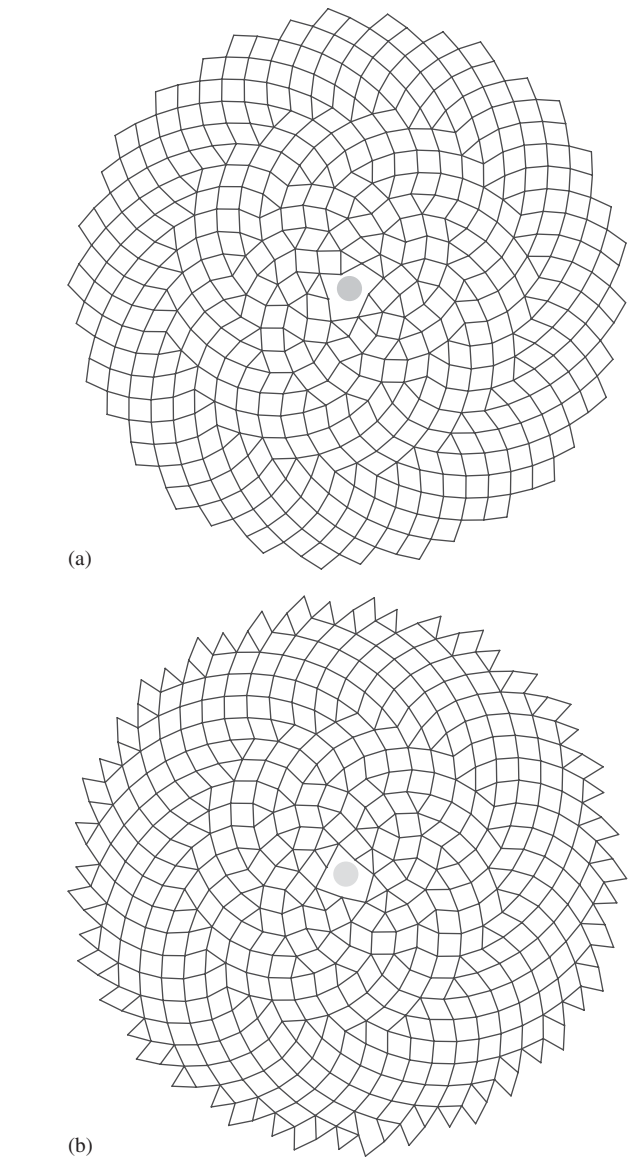Fig. 12. Spiral-pattern resulting from Hofmeister's rule with LCVR, $n = 500$, movement limit: 0.3, relaxation depth: 10, $\varepsilon = 0.01$. (a) Fibonacci-spiral (starting angle 125°). (b) Lucas-spiral $(18, 29, 47, \ldots)$ (starting angle: 55°).

Appendix A. Ridley's contact pressure algorithm

A.1. Ridley's calculation of the interaction of the primordia

After inserting a new primordia and before expanding the whole capitulum the following interaction procedure is carried out a number m of times (we call this number the wave number of relaxation steps). Remark that zyklus is the index of the youngest primordia and that the oldest primordia has index one.

Input
Number of relaxing-steps m
Move limit ℓ
begin
   for wave = 1 **to** m **do**
   begin

```
   for i = zyklus downto 1 do
   begin
      moveSum(i) = 0, move(other,i) = 0, move(i) = 0
      for other = zyklus downto 1 do
      begin
         if (other ≠ i) and (dist(P(other) − P(i)) < 2)
         then calculate move(other,i) (see Eq. (A.1))
         moveSum(i) = moveSum(i) + move(other,i)
         end (for other)
      calculate move(i) (see Eq. (A.2))
      restrict move(i) if necessary
      P(i) = P(i) + move(i)
   end (for i)
 end (for wave)
end.
```
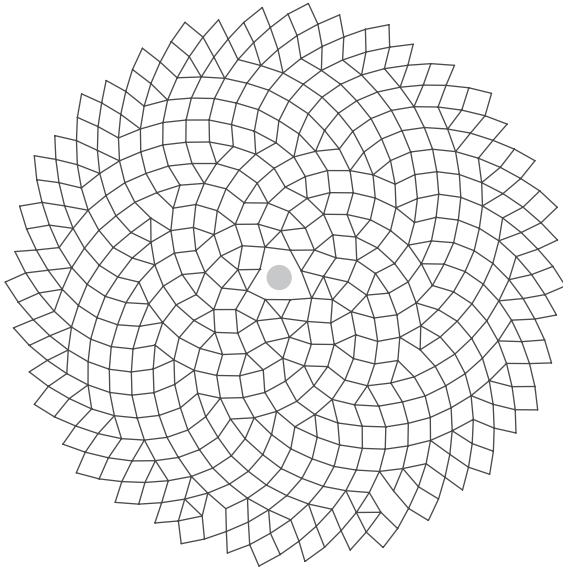
Fig. 13. Main Fibonacci bijugy $(2, 4, 6, 10, 16, 26, 42, \ldots)$ resulting from Hofmeister's rule with LCVT, $n \approx 500$ (starting angle $105°$, movement limit: $0, 3$, relaxation depth: 10, $\varepsilon = 0.01$).
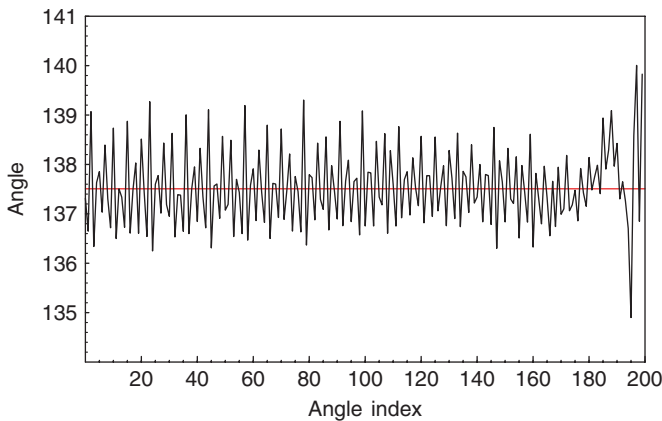

Fig. 14. Divergence angle between the first two youngest primordiain capitula (200 primordia) resulting from a contact pressure simulation with LCVR (3 waves, movement limit $0, 3$) and Hofmeister rule (starting angle: $125°$, input with SD $3, 6°$).

A.2. Ridley's calculation of contact pressure movements

The displacement vector $\overrightarrow{move(i,j)}$ resulting from the application of the contact pressure of the primordium P_j to primordium P_i is computed by Ridley (1982) in the following way: if the distance $k := dist(P_i, P_j)$ between the centers of the two primordia is less than 2 (we will call such a P_j a neighbor of P_i) than for the pair (P_i, P_j) a displacement vector $\overrightarrow{move(i,j)}$ is calculated which would P_i shift in direction of the difference vector $\overrightarrow{P_i} - \overrightarrow{P_j}$ into a position $\tilde{P}_i$ with distance $D = 1 + \frac{1}{2}k$ to P_j.

Please note that $\overrightarrow{move(i,j)}$ will be calculated but not

executed. So

$$\overrightarrow{move(i,j)} = \left(\frac{1}{k} + 0.5\right)(\overrightarrow{P_i} - \overrightarrow{P_j}) - \overrightarrow{P_i}. \tag{A.1}$$

A simple calculation shows that this is an approximation of the movement of two intersecting discs to each of their centroids. This is done analogously for all other neighbors of P_i. After doing so, the arithmetic mean of all neighbor movements is computed:

$$\overrightarrow{move(i)} = \frac{1}{N_i} \sum_j \overrightarrow{move(i,j)}, \tag{A.2}$$

where N_i is the number of neighbors P_j of P_i. It is important to remark that this mean is an inexact measure for the resulting movement since the influences of all neighbors is weighted equally which is not the case for real primordia.

Before adding the displacement vector $\overrightarrow{move(i)}$ to $\overrightarrow{P_i}$ Ridley applies some restrictions which should reflect the restrictions of movements on cell tissues provided by the underlying biology:

(1) only a movement less than ℓ (Ridley choose $\ell = 0.1$) units is carried out, meaning if $|\overrightarrow{move(i)}| \geqslant \ell$ than we apply the movement

$$(\overrightarrow{move(i)}/|\overrightarrow{move(i)}|) \cdot \ell. \tag{A.3}$$

(2) the distance of primordium P_i from the center must always be between $\sqrt{i - 1/2}$ and $\sqrt{i + 1/2}$.

Then the new position resulting from the contact pressure is computed by

$$\overrightarrow{P_i} = \overrightarrow{P_i} + \overrightarrow{move(i)}. \tag{A.4}$$

This is done for all exciting primordia from the youngest to the eldest.

Appendix B. Centroidal Voronoi tessellation (CVT)

For a given domain $\Omega \subset \mathbb{R}^d$ a Voronoi tessellation associate with a given generator point set $S = \{p_i\}_{i=1}^n \subset \Omega$ is the disjoint partition of Ω in Voronoi regions $\{V_i\}_{i=1}^n$ of nearest neighborhood according to a given metric. In the following we use the Euclidian metric $\| \cdot \|_2$ for our computations.

The Voronoi regions that are generated from $p_i \in S$ can be described by

$$V_i = V(p_i, S) = \bigcap_{p_j \in S \setminus \{p_i\}} \{p \in \mathbb{R}^d : \|p_i - p\|_2 < \|p_j - p\|_2\}. \tag{B.1}$$

I.e. the Voronoi regions are the intersections of a number of half-spaces that describe the regions where points $p \in \mathbb{R}^d$ have a smaller distance to point p_i than to another point p_j.

For a given density function ρ on Ω the centroids $\{p_i^*\}_{i=1}^n$ of the Voronoi regions $\{V_i\}_{i=1}^n$ are defined by

$$p_i^* = \frac{\int_{V_i} y \cdot \rho(y)\,\mathrm{d}y}{\int_{V_i} \rho(y)\,\mathrm{d}y}. \qquad (B.2)$$

A centroidal Voronoi tessellation is a Voronoi tessellation for which the generators themselves are the centroids of their respektive Voronoi regions, that mean $p_i^* = p_i$ for all i. For a comprehensive review of CVTs cf. Du et al. (1999).

B.1. The Lloyd-algorithm

A simple algorithm for computing a CVT is the Lloyd-algorithm. It is an iterative algorithm consisting of the following steps: first select a threshold ε and a upper limit of cycles (we call this number the relaxation depth).

(1) For a given generator point set $S = \{p_i\}_{i=1}^n \subset \Omega$ compute the Voronoi regions $\{V_i\}_{i=1}^n$.
(2) Calculate the centroids $\{p_i^*\}_{i=1}^n$ of the Voronoi regions $\{V_i\}_{i=1}^n$ and

$$\text{maxdist} = \max_{i=1,..,n}(\text{dist}(p_i, p_i^*)). \qquad (B.3)$$

(3) Move the generator points p_i to the centroids p_i^*.
(4) Repeat steps (1)–(3) until maxdist $< \varepsilon$ or the upper limit of cycles is reached.

B.2. Contact pressure calculation with the LCVR

Input
 Relaxation depth m
 Threshold ε
 Move limit ℓ
begin
 wave $= 0$
 repeat
 wave $=$ wave $+$ 1
 for i $= 1$ **to** zyklus **do**
 begin
  calculate $V(i)$ and the centroid p_i^*
  calculate $\text{dist}(p_i, p_i^*)$ and $\overrightarrow{move(i)}$ as the difference vector $\overrightarrow{p_i^*} - \overrightarrow{p_i}$
  restrict $\overrightarrow{move(i)}$ if necessary
 end (**for** i)
 calculate maxdist (see Eq. (B.3))
 for i $= 1$ **to** zyklus **do** $\overrightarrow{P(i)} = \overrightarrow{P(i)} + \overrightarrow{move(i)}$
 until ((maxdist $< \varepsilon$) **or** wave $=$ m)
end.

References

Adler, I., 1974. A model of contact pressure in phyllotaxis. J. Theor. Biol. 45 (1), 1–79.

Adler, I., 1975. A model of space filling in phyllotaxis. J. Theor. Biol. 53, 435–444.

Adler, I., 1998. The role of continued fractions in phyllotaxis. J. Algebra 205, 227–243.

Adler, I., Barabe, D., Jean, R.V., 1997. A history of the study of phyllotaxis. Ann. Bot. 80, 231–244.

Atela, P., Gole, C., Hotton, S., 2002. A dynamical system for plant pattern formation. J. Nonlinear Sci. 12 (6), 641–676.

Bashein, G., Detmer, P.R., 1994. Centroid of a polygon. In: Heckbert, P.S. (Ed.), Graphic Gems, vol. IV. Morgan Kaufmann, Los Altos, CA, pp. 3–8.

Bernasconi, G., 1994. Reaction–diffusion model for phyllotaxis. Physica D 70, 90–99.

Coxeter, H.S.M., 1972. The role of intermediate convergents in Taits explanation for phyllotaxis. J. Algebra 20, 167–175.

Dixon, R., 1983. The mathematics and computer graphics of spirals in plants. Leonardo 16 (2), 86–90.

Dixon, R., 1998. The shape of Dirichlet regions in a coxeter lattice as a function of divergence and rice. In: Jean, R.V., Barabe, D. (Eds.), Symmetry in Plants. Series in Mathematical Biology and Medicine, vol. 4, Singapore, pp. 313–333.

Douady, S., Couder, Y., 1996. Phyllotaxis as a dynamical self organizing process (Part I, II, III). J. Theor. Biol. 178, 255–312.

Du, Q., Faber, V., Gunzburger, M., 1999. Centroidal Voronoi tessellations. SIAM Rev. 41 (4), 637–676.

Flemming, A.J., 2005. Formation of primordia and phyllotaxy. Curr. Opin. Plant Biol. 8, 53–58.

Hofmeister, W., 1886. Allgemeine Morphologie der Gewächse. In: Handbuch der Physiologischen Botanik, vol. 1, Leipzig, pp. 405–664.

Honda, H., 1978. Description of cellular patterns by Dirichlet domains. The two dimensional case. J. Theor. Biol. 72 (3), 523–543.

Honda, H., 1983. Geometrical modelling of cells in tissues. Inter. Rev. Cytol. 81, 191–248.

Jean, R.V., 1994. Phyllotaxis. Cambridge.

Jean, R.V., Barabe, D. (Eds.), 1998. Symmetry in Plants. Series in Mathematical Biology and Medicine, vol. 4, Singapore.

Khinchin, A. Ya., 1964. Continued Fractions. Chicago.

Koch, A.-J., Bernasconi, G., Rothen, F., 1998. Phyllotaxis as a geometrical and dynamical system. In: Jean, R.V., Barabe, D. (Eds.), Symmetry in Plants. Series in Mathematical Biology and Medicine, vol. 4, Singapore, pp. 459–486.

Kuhlemeier, C., Reinhardt, D., 2001. Auxin and phyllotaxis. Trends Plant Sci. 6 (5), 187–189.

Marzec, C., Kappraff, J., 1983. Properties of maximal spacing on a circle. J. Theor. Biol. 103, 201–226.

Meinhardt, H., 2003. Complex pattern formation by a self-destabilization of established patterns. C. R. Biol. 326 (2), 223–237.

Richards, F.J., 1948. The geometry of pyllotaxis and its origin. Symp. Soc. Exper. Biol. 2, 217–245.

Ridley, J.N., 1982. Computer simulation of contact pressure in capitula. J. Theor. Biol. 95, 1–11.

Ridley, J.N., 1986. Ideal phyllotaxis on a general surface of revolution. Math. Biosci. 79, 1–24.

Rivier, N., Occelli, R., Pantaloni, J., Lissowski, A., 1984. Structure of Bernard convection cells, phyllotaxis and crystallography in cylindrical symmetry. J. Phys. 45, 49–63.

Rothen, F., Koch, A.-J., 1989. Phyllotaxis, or the properties of spiral lattices I. J. Phys. France 50, 633–657.

Ryan, W., Rouse, J.L., Bursill, L.A., 1991. Quantitative analysis of sunflower seed packing. J. Theor. Biol. 147, 303–328.

Schoute, J.C., 1913. Beiträge zur Blattstellungslehre I. Die Theorie. Rec. Trav. Bot. Neerl. 10, 153–339.

Schoute, J.C., 1938. Early binding whorls. Rec. Trav. Bot. Neerl. 35, 416–558.

Schwendener, S., 1878. Mechanische Theorie der Blattstellungen. Engelmann, Leipzig.

Snow, M.R., 1952. Minimum areas and leaf determination. Proc. Roy. Soc. London 139B, 545–566.

Snow, R., 1955. Problems of phyllotaxis and leaf determination. Endeavour 14, 190–199.

Stieger, A., Reinhardt, D., Kuhlemeier, C., 2002. The auxin influx carrier is essential for correct leaf positioning. Plant. J. 32, 509–517.

Turing, A.M., 1992. In: Saunders, P.T. (Ed.), Morphogenesis. Collected Works of A.M. Turing. North-Holland, Amsterdam [u.a.].

van Ravenstein, T., 1989. Optimal spacing of points on a circle. Fibonacci Quart. 27, 18–24.

Vogel, H., 1979. A better way to construct the sunflower head. Math. Biosci. 44, 179–189.

Williams, R.F., Brittain, E.G., 1984. A geometrical model of phyllotaxis. Aust. J. Bot. 32, 43–72.